Hindawi
Geofluids
Volume 2022, Article ID 4093526, 13 pages
https://doi.org/10.1155/2022/4093526

Research Article

Mechanical Behaviors and AE Characteristics of Brittle Coal Specimens with Different Fissure Angles

Xuebin Gu,[1] Weiyao Guo,[1,2] Chengguo Zhang,[1,2,3] Chuanqing Guo,[4] Chao Wang,[5] Fangfang Wang,[5] Tongbin Zhao,[1] and Yang Chen[6]

[1]*College of Energy and Mining Engineering, Shandong University of Science and Technology, Qingdao 266590, China*
[2]*State Key Laboratory of Mining Disaster Prevention and Control Co-founded by Shandong Province and the Ministry of Science and Technology, Shandong University of Science and Technology, Qingdao 266590, China*
[3]*School of Minerals and Energy Resources Engineering, UNSW Sydney, Sydney, Australia*
[4]*Yankuang Energy Group Co., Ltd., Jining No. 2 Coal Mine, Jining 272012, China*
[5]*Yankuang Energy Group Co., Ltd., Jining 273500, China*
[6]*Shandong Energy Group Co., Ltd., Jinan 250014, China*

Correspondence should be addressed to Weiyao Guo; 363216782@qq.com and Chengguo Zhang; zhchengguo@gmail.com

Received 3 June 2022; Revised 27 July 2022; Accepted 10 August 2022; Published 22 September 2022

Academic Editor: Quanle Zou

Uniaxial compression tests were performed on coal specimens with five fissure angles to study the mechanical behaviors and acoustic emission (AE) characteristics of fractured coals. AE and video monitoring techniques were used to examine crack propagation in the fractured specimens. The stress–strain curves, mechanical properties, and cracking processes at different fissure angles were analysed. The AE counts and dominant frequency characteristics, during the failure processes of the specimens, were investigated. In addition, five types of AE signals were classified according to the AE spectral frequency analysis, and low-frequency–high-energy signals were used to accurately predict the brittle fracture processes of the fractured specimens. Finally, a comparison with sandstone specimens revealed the influence of primary cracks on the strength of brittle coal specimens containing preexisting fissures under uniaxial compression. The test results are helpful to elucidate the mechanical behavior and failure mechanism in underground engineering, such as hydraulic slotting in mines.

1. Introduction

Several joints, fissures, and structural planes exist in rock masses because of geological tectonics and mining activities [1–3]. Crack propagation and coalescence are the primary reasons for the failure of engineering rock masses, which may cause dynamic instability of the roadway [4–8]. Therefore, research on the crack propagation and failure characteristics of jointed rock materials is necessary to clarify the failure mechanism of fractured rocks.

Researchers have conducted experimental and numerical investigations on fractured rocks. Several experimental laboratory studies have focused on the influence of the geometric distribution of preexisting flaws on crack propagation in prefabricated rock specimens ([9–12]). Wong and Einstein [13, 14] investigated the effects of different flaw geometries (inclination angle, ligament length, and bridging angle) and materials on the cracking process. Yang and Jing [15] performed uniaxial compression tests on sandstone containing a preexisting flaw and investigated the effects of the flawed layout using deformation and failure characteristics. Morgan et al. [16] studied the cracking and coalescence behavior of granite specimens with preexisting flaw pairs and recorded the cracking process using a high-speed

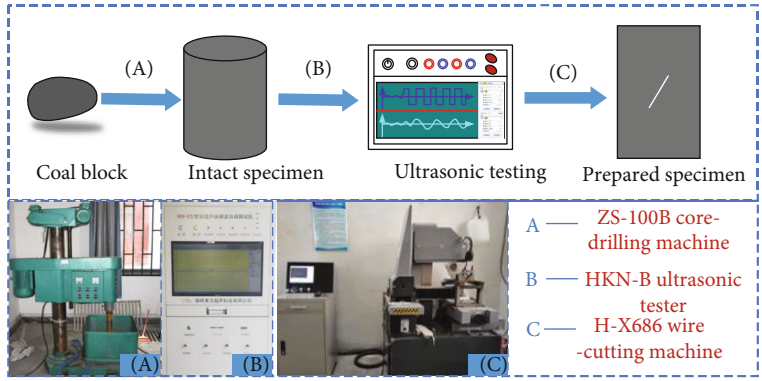

(a) Specimen preparation

(b) Coal specimen with prefabricated fissures

Figure 1: Flowchart of preparation of specimens.

camera. Dou et al. [17] investigated the influence of the crack dip angle on the fracture mechanism of sandstone specimens under uniaxial compression tests. Zhou et al. [18] studied the progressive cracking process in granite under uniaxial loading using digital imaging and AE techniques. Uniaxial loading tests were conducted to evaluate the effect of the loading mode. Haeri et al. [19] performed Brazilian splitting tests on precracked disk specimens. Yu et al. [20] studied the mechanical characteristics of sandstone specimens with different loading rates and analysed the effect of the loading rate on the failure mechanism. Xiao et al. [21] tested the crack growth and strength of specimens with precracks under triaxial loading and analysed their failure mechanisms.

Numerical simulations are often performed because they are repeatable and can provide valuable information regarding internal cracks and mechanics [22–25]. For example, Bahaaddini et al. [26] used particle flow code (PFC^{3D}) to investigate the effects of the geometric parameters of joints on the rock-mass failure mechanism. Wong and Li [27] numerically simulated the coalescence of two preexisting coplanar flaws in rocks under compression conditions. Lee et al. [28] investigated the mechanism of fracture coalescence in precracked rock-type material with three flaws. Zhao et al. [29] simulated the coalescence modes of two preexisting parallel cracks using a universal distinct element code (UDEC). Huang et al. [30] combined laboratory tests and PFC to study the fracture mechanism of a preexisting crack with a large opening and found that the failure of these large-opening crack specimens was primarily caused by the development of shear secondary cracks instead of tensile wing cracks.

Previous studies have primarily focused on the mechanical properties and crack propagation characteristics of rocks and rock-like materials. Few studies have investigated the crack propagation and AE characteristics of fractured coal, and most have used coal-like materials instead of coal [31–34]. For example, Zhang et al. [35] used gypsum instead of soft coal to investigate the deformation energy density characteristics and failure mechanism of coal samples with single fissures at different inclination angles. Jin and Lian [36] studied the influence of prefabricated fissures on the coal burst liability and failure behavior through numerical simulations. If a laboratory test of a real coal specimen is conducted, the failure essence of the fractured coal will be better explained.

Therefore, to better understand the strength, crack-coalescence phenomenon, and AE characteristics of brittle coal materials, uniaxial compression experiments were conducted on coal specimens containing a single fissure. Moreover, AE and video monitoring techniques were used to examine crack propagation in the fractured specimens. The results are expected to provide a basis for the study of the mechanical properties and failure mechanisms of fractured coal.

2. Specimen Preparation and Testing Process

2.1. Specimen Preparation. All the specimens were obtained from a working face in a mine located in western China.

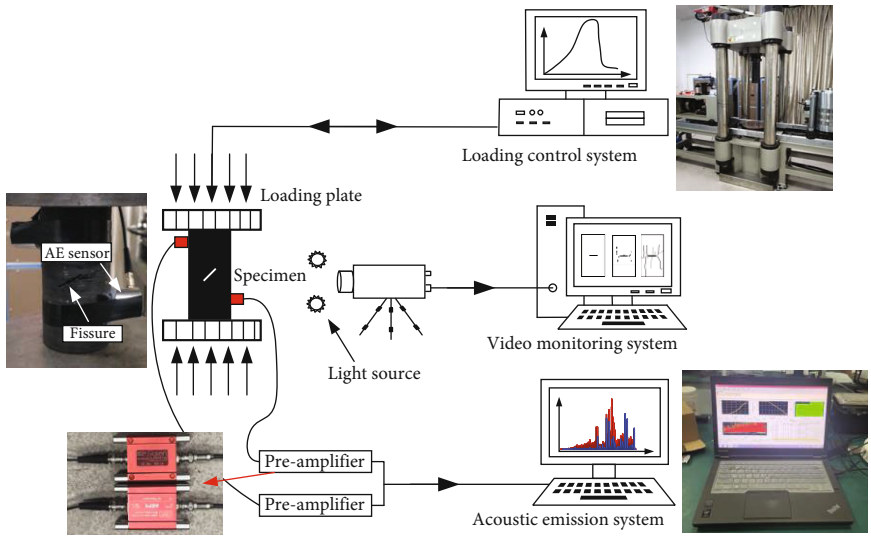

Figure 2: Experimental system.

After sampling, coal with a large block size was delivered to the laboratory as standard-specimens, shown in Figure 1(a). First, a cylindrical coal specimen with a diameter of 50 mm and a height of 100 mm was acquired using a core-drilling machine and a cutting machine. To further comply with international rock-testing standards, the ends of the specimen were polished meeting the parallelism standard such that the parallelism of the end face is within ±0.02 mm, and the end diameter deviation is less than 0.02 mm. Then, the *P*-wave velocity test was carried out on the coal specimens to avoid discreteness of the test results; specimens with similar density and *P*-wave velocity were selected for the next test. Finally, according to a previously reported fissure manufacturing method [37], round holes with small diameters were first prefabricated using a mechanical machining method, and then, a line cutting machine was used to cut through the small holes along the fissure direction.

Three geometrical characteristics determine the fissure geometry: fissure length $2l$, fissure width d, and fissure angle α. Specimens with five fissure angles were prepared ($\alpha = 0^\circ$, 15°, 30°, 45°, and 60°), and the fissure length and width were 20 and 1 mm, respectively. The specimens were labelled according to their fissure angles. For instance, 0°-1 represents the first specimen with a fissure angle of 0°.

2.2. Testing System and Process. As shown in Figure 2, the experimental system included a loading system, an AE monitoring system, and a video monitoring system. Uniaxial tests were performed using RLJW-2000 rock-testing equipment with an AMSY-6 AE system [38]. In this test, the loading rate was 0.25 mm/min. The sampling frequency of the AE system was 10 MHz, and the recording threshold was 40 dB. Two AE sensors were installed on each side of the specimen along the radial direction, and Vaseline was used to enhance the coupling effect. An EOS C100 camera was used to capture images when a macrocrack or failure occurred.

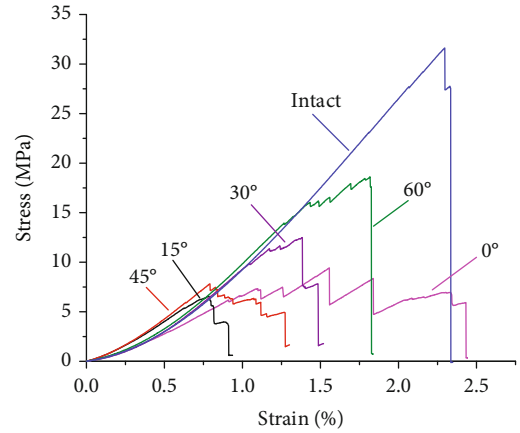

Figure 3: Stress–strain curves of specimens with different fissure angles.

3. Results and Analysis

3.1. Stress–Strain Curves and Mechanical Behaviors. Figure 3 presents the stress–strain curves of the specimens containing preexisting fissures with different fissure angles. The intact specimen exhibited a higher uniaxial strength compared to fractured specimens. Stress–strain behavior can be divided into four typical stages: compaction, elastic deformation, crack growth and propagation, and strain softening. Preexisting fissures reduce the elastic stage duration and clearly affect crack growth and propagation as well as strain softening. However, the stress–strain curves at different fissure angles did not exhibit obvious variation rules. All analyses indicated that the fissure angle significantly affected the stress–strain curve and mechanical properties.

Table 1 presents the uniaxial compressive stress (UCS), elastic modulus (E), and axial strain of the peak stress (peak strain) for the specimens in the uniaxial compressive tests.

Table 1: Mechanical parameters of the specimens under uniaxial compression tests.

Number	UCS/ MPa	Average/ MPa	Standard deviation	E/ GPa	Average/ GPa	Standard deviation	Peak strain/ %	Average/ %	Standard deviation
a-1	31.62	32.8	1.1800	1.76	1.74	0.0200	2.30	2.39	0.0882
a-2	33.98			1.72			2.47		
0°-1	10.16			0.7			2.46		
0°-2	9.43	9.55	0.4570	0.85	0.83	0.0990	1.56	1.77	0.5000
0°-3	9.06			0.94			1.30		
15°-1	6.38	6.47	0.0900	1.07	1.06	0.0050	0.79	0.79	0.0042
15°-2	6.56			1.06			0.78		
30°-1	12.14			1.10			1.68		
30°-2	13.19	12.60	0.4374	1.31	1.25	0.1040	1.52	1.53	0.1209
30°-3	12.48			1.33			1.38		
45°-1	9.03			1.20			0.98		
45°-2	7.56	8.14	0.6405	1.18	1.19	0.0094	0.84	0.87	0.0780
45°-3	7.82			1.20			0.79		
60°-1	18.61			1.53			1.82		
60°-2	15.79	16.4	1.6112	1.5	1.46	0.0741	1.55	1.65	0.1199
60°-3	14.81			1.36			1.58		

Figure 4 shows the curves of these parameters with respect to the fissure angle.

As shown in Figure 4(a), the UCS did not exhibit an evident trend with an increase in the fissure angle, which may be closely related to the primary fractures in the coal. Compared to the UCSs of the intact specimens, those of the fractured specimens decreased by 70.88%, 80.27%, 61.59%, 75.18%, and 50% at fissure angles of 0°, 15°, 30°, 45°, and 60°, respectively. As shown in Figure 4(b), with an increase in the fissure angle, the elastic modulus ranged from 0.83 to 1.74 GPa with an increasing trend except for the fissure angle of 45°. The elastic modulus reached the minimum value of 0.83 GPa when the fissure angle was 0°. Figure 4(c) shows the relationship between the peak strain and fissure angle. As the fissure angle increase, the peak strain does not exhibit a specific trend. The peak strains of the fractured specimens were smaller than those of the intact specimens. This was because the fissures destroyed the specimens, resulting in their failure at a small axial strain.

3.2. Crack Evolution Process. A video monitoring system was used to investigate the crack evolution in the fractured specimens subjected to uniaxial compressive tests. The process of crack coalescence, according to the results of stress and photographic monitoring, is shown in Figure 5. Specimens with fissure angles of 0°, 30°, and 60° were selected for subsequent analysis.

Figure 5(a) shows the stress–strain curve of the specimen with a fissure angle of 0° and the corresponding crack-propagation sketch. During the compaction and elastic deformation stages, owing to the low degree of stress concentration near the fissure, no crack initiation was observed around the preexisting fissure. When the stress reached point a ($\sigma = 5.17$ MPa), two small cracks extended from the centre of the fissure. With an increase in axial stress, the cracks widened significantly, and the preexisting fissure began to close. At point c ($\sigma = 7.34$ MPa), a new tensile crack is rapidly generated at the left tip of the fissure, resulting in a minor stress drop. The fissure disappeared from view. When the specimen was loaded at 7.49 MPa (point d), two cracks were generated at the tip of the fissure and propagated in the axial-stress direction. As the deformation increased, more cracks appeared which reduced the axial supporting capacity.

Figure 5(c) shows the stress–strain curve of the specimen with a fissure angle of 30° and the corresponding crack propagation sketch. The stress drop in the stress–strain curve indicates macrocrack propagation. When the axial stress reached 9.61 MPa (point a), cracks 1 and 2 initiated at the tip of the fissure in the wing of the specimen. When the stress increased to 12.22 MPa (point e), crack 3 emerged from the upper tip of the fissure and grew in the loading direction, exhibiting an "H" pattern. At point f, the preexisting fissure was completely closed. When the specimen was loaded to point g ($\sigma = 7.83$ MPa), cracks developed at the boundary and the specimen expanded significantly, leading to a sharp decline in the bearing capacity.

Figure 5(e) shows the stress–strain curve of the specimen with a fissure angle of 60° and the corresponding crack propagation sketch. As indicated by the sketch, macrocracks developed around the fissure from point a ($\sigma = 13.95$ MPa) to point c ($\sigma = 16.04$ MPa) leading to several stress fluctuations. Particle ejection and fissure closure were observed at point d (16.15 MPa). When the specimen was loaded to 18.61 MPa (point g), ejection occurred once more, resulting in a rapid decline in the axial stress.

The stress–strain curves reflected the macroscopic crack growth of the fractured specimens, and the stress drop generally corresponded to significant macroscopic crack growth. The initial crack appeared at the centre of the preexisting fissure and at the tip of the fissure. When the fissure angle was 0°, crack initiation occurred at the centre of the preexisting

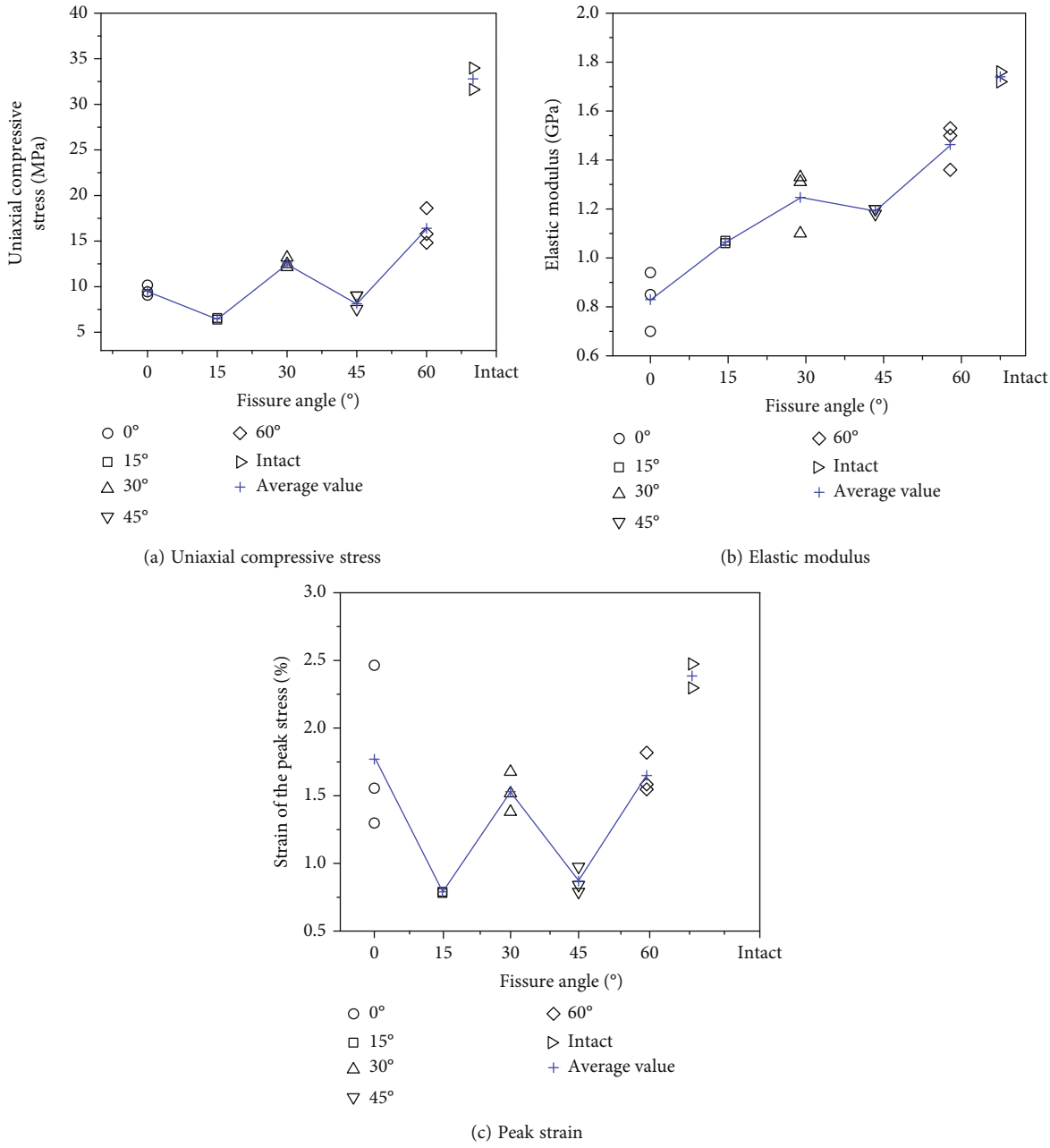

(a) Uniaxial compressive stress

(b) Elastic modulus

(c) Peak strain

Figure 4: Curves of the UCS, elastic modulus, and peak strain with respect to the fissure angle.

fissure. With a greater fissure angle, the crack-initiation location moved to the tip. The crack propagated along the loading direction, indicating that the fissure angle did not significantly affect the direction of crack development.

3.3. AE Counts and Energy. AEs refer to the elastic waves released by the internal damage of a rock specimen. The AE count is the number of waves in which an AE signal exceeds the threshold, and AE energy refers to the area under the detection envelope of the AE signal. These parameters are useful for investigating the failure processes and crack-coalescence mechanisms of flawed specimens with different fissure angles [39–42]. Figure 6 shows the curves of stress, AE count, and AE energy with respect to time in the uniaxial compression tests. The AE characteristics of the specimens can be divided into three typical periods: calm period (I), active period (II), and remission period (III).

Using a fissure angle of 0° as an example, the AE characteristics of the three periods were analysed, as shown in Figure 7(a). During the calm period, the axial stress was small, and few AE activities were monitored. This was because the closure of the primary cracks was a small-scale rupture, and the AE counts and energy were low. This period corresponded to the compaction stage and part of the elastic-deformation stage. During the active period, with an increase in the loading stress, more cracks initiated and propagated. Therefore, the AE counts and AE energy of the fractured specimens increased and exhibited multiple

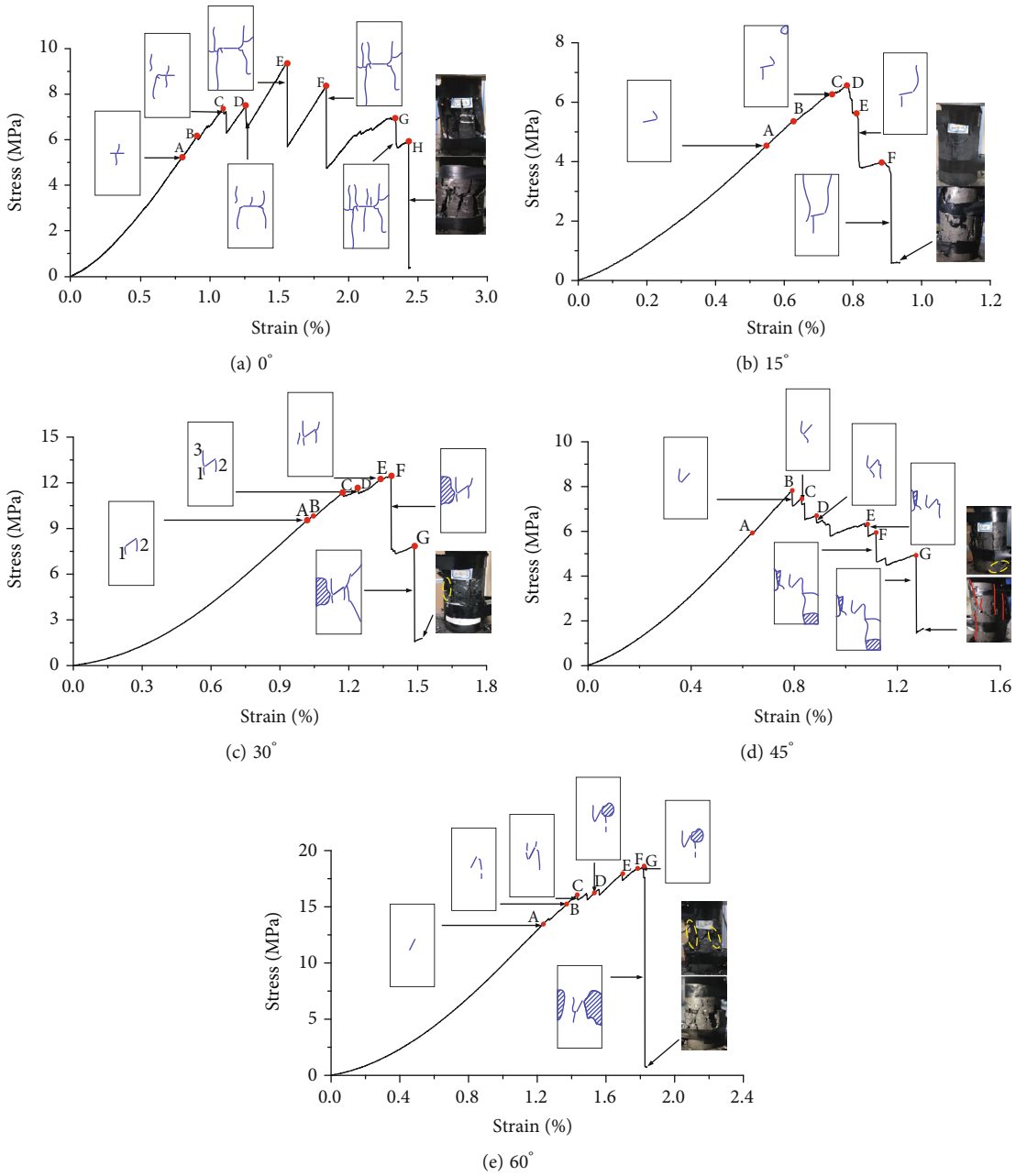

Figure 5: Relationship between the crack propagation and the stress–strain curve for typical specimens.

peaks during the prepeak stage. The absence of signals in the time period of 400–600 s likely resulted from the propagation of axial cracks. During the remission period, the axial stress decreased to a low level, and AE activity seldom appeared.

In summary, the AE counts and energy characteristics of the fractured specimens varied among different cracking stages. The duration proportion of the calm period increased with an increase in the fissure angle, indicating that the evolution characteristics of AE were different for different fissure angles.

3.4. AE Spectrum Frequency Characteristics. The frequency spectra reflect important characteristics of the AE signal and can provide insightful quantitative information regarding the cracking process [43, 44]. In addition, AE energy can be used to determine the scale of the rock rupture. Combining these two parameters can provide a better understanding of crack propagation. The dominant frequencies of the AE signals were calculated using the Fourier transform. AE energy was determined using a parametric analysis method.

Figure 7 shows the AE frequency–energy characteristic diagram of the failure process. Evidently, the dominant

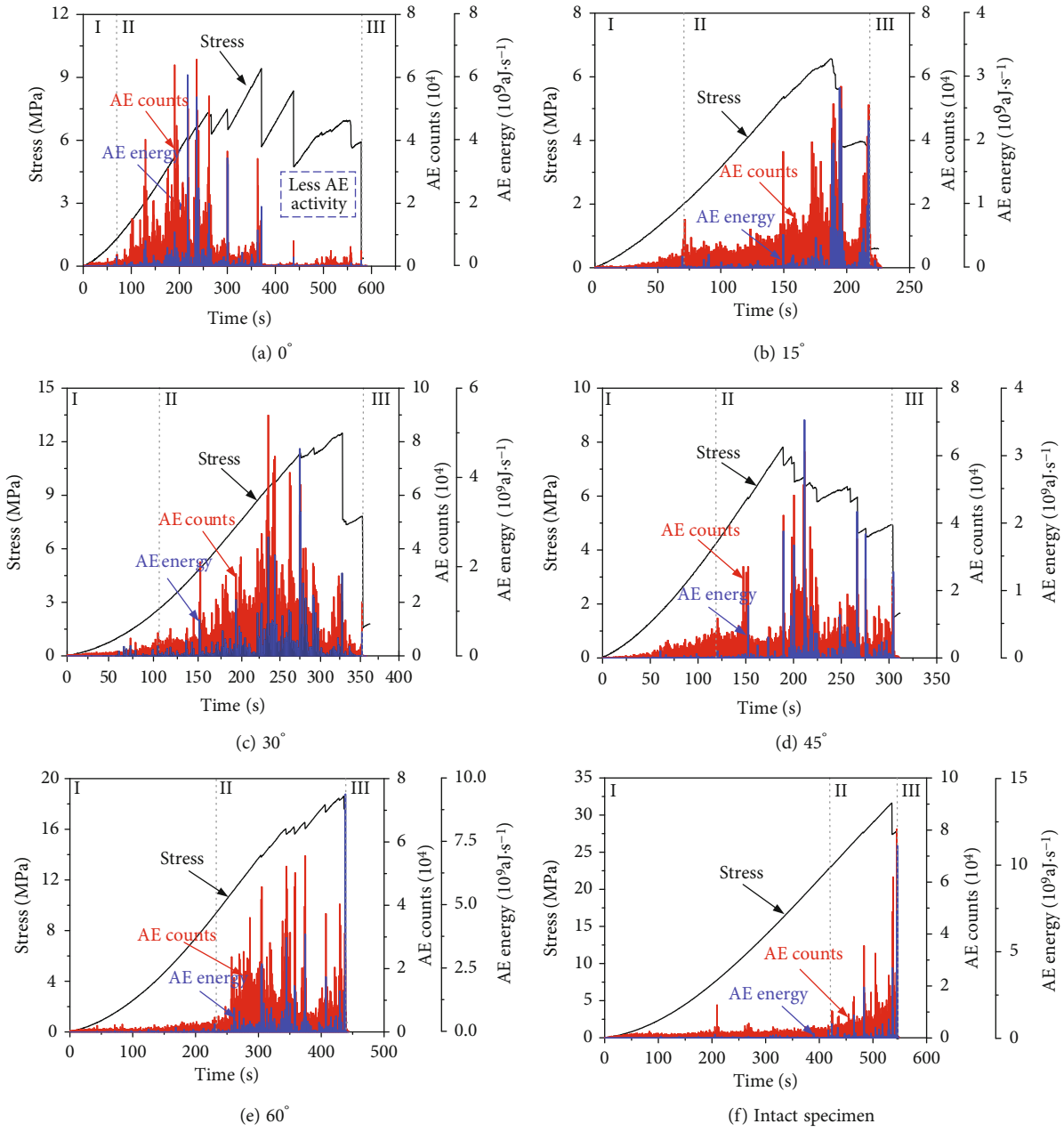

Figure 6: AE characteristics of specimens with different fissure angles.

frequency of the specimen presented a similar evolution law with a dense band-like evolution. Based on the frequency distribution, three main frequency bands were identified: low [0, 125], medium [125, 225], and high [225, 325]. A fissure angle of 0° was used as an example to investigate the main frequency–energy evolution characteristics of the specimen. During the initial stage of loading, the signal was concentrated in the frequency ranges of 25–125 kHz and 150–200 kHz; the signal energy in most loading stages was $<10^6$ aJ. As the loading continued, high-frequency signals with a main frequency of 300 kHz appeared. Simultaneously, numerous high-energy signals with energy levels $> 10^7$ aJ appeared between 25 kHz and 125 kHz and near 100 kHz, which corresponded well to the stress drop. After the stress peak, the number of AE signals decreased significantly, which may be related to the development of axial macroscopic cracks. A comparison of the evolution characteristics of the dominant frequency at different fissure angles evealed that the number of signals in the ranges 50–75 kHz and 150–200 kHz tended to decrease with an increase in the fissure angle.

Apart from the changes in the dominant frequency during the failure process, the examination of the AE energy distribution makes it possible to further explore the failure law of brittle coal. The dominant frequency and energy for the fractured coal specimens are plotted in Figure 8. Evidently, high-energy events were mainly distributed in the low-frequency band [0, 125]. The signals are divided into two types based

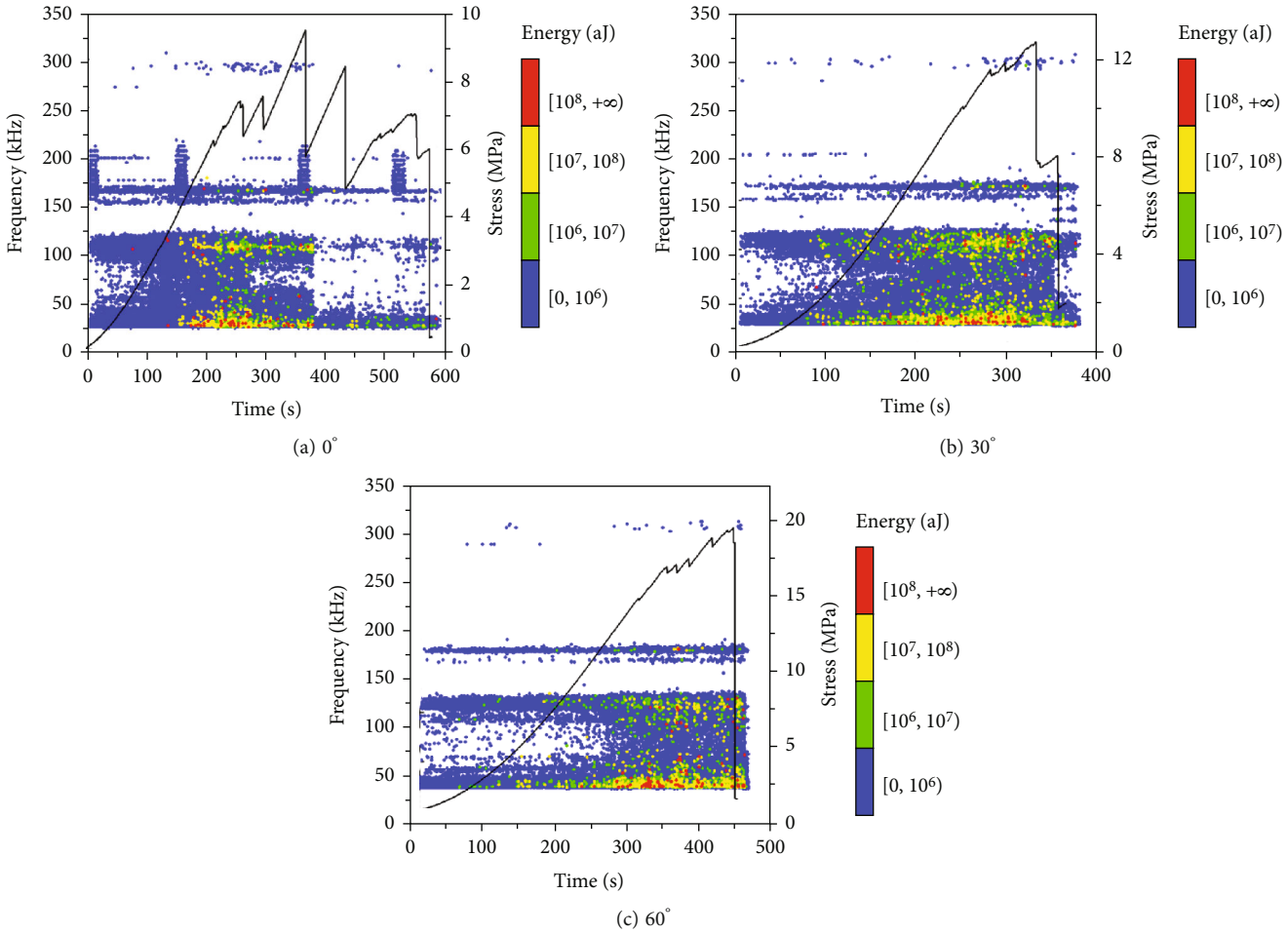

Figure 7: Frequency–energy characteristics of the failure process.

on their energy. Signals with an energy magnitude > 10^7 aJ were classified as high-energy, and those with energy magnitudes < 10^7 aJ were classified as low-energy.

Combined with the main frequency characteristics in Figure 7, five types of AE signals were observed: low-frequency–low-energy (L-L), low-frequency–high-energy (L-H), medium-frequency–low-energy (M-L), medium-frequency–high-energy (M-H), and high-frequency–low-energy (H-L) signals. Based on the relationships between the crack type, size, and domain frequency, the following conclusions were drawn: (1) L-L and M-L signals appeared in the early stage of loading, which may have been related to the fracture of the crystal particles. (2) A few L-H signals mostly appeared near the stress-reduction point, indicating that they were generated by large macroscopic cracks. (3) A few M-H signals were concentrated at the failure phase; this may have been related to the block slip in the preexisting flaw area. (4) In the crack growth and propagation stage, five types of AE signals coexisted, indicating that microcrack initiation, microcrack extension, and macrocrack propagation occurred simultaneously. (5) The failure of the specimen involved the process of microcrack initiation, development, expansion, and macrocrack penetration. Owing to their relationship with macrocracks, L-H signals can be used to predict the brittle fracture states of fractured coal specimens.

4. Discussion

4.1. Strength Characteristics of Specimens with Different Fissure Angles. The experimental results indicated that the strengths of the fractured coal specimens exhibited no specific law with an increase in the fissure angle. The uniaxial compressive strengths and elastic moduli concerning the specimens containing preexisting fissures were lower compared to intact specimens. Yang and Jing [15] performed uniaxial compressive tests on sandstone with different fissure angles and found that the strength was minimized at a fissure angle of 45°. This conclusion differs from the experimental results of this study. Compared to the sandstone specimens, the coal material contained more primary cracks, and the combined effects of the preexisting fissure and primary cracks may have led to irregular strength changes.

Preexisting fissures can be regarded as defects that reduce the integrity of a specimen and significantly reduce its strength. When a compression load was applied to the fractured coal specimens, stress concentration first occurred

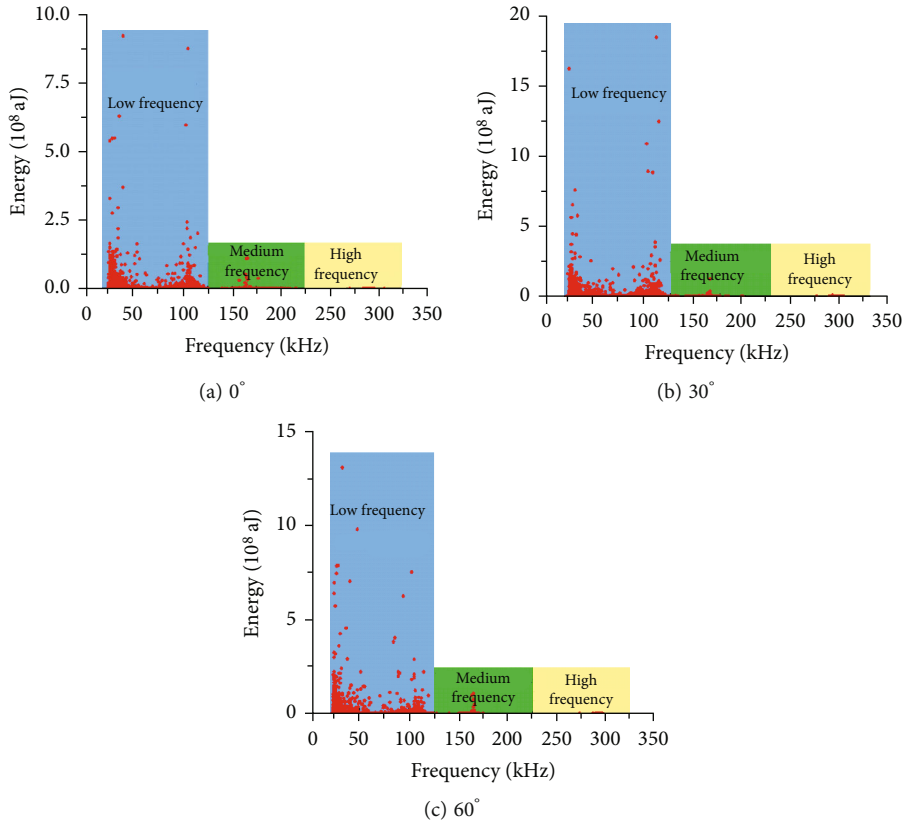

Figure 8: Relationship between the dominant frequency and energy for fractured coal specimen.

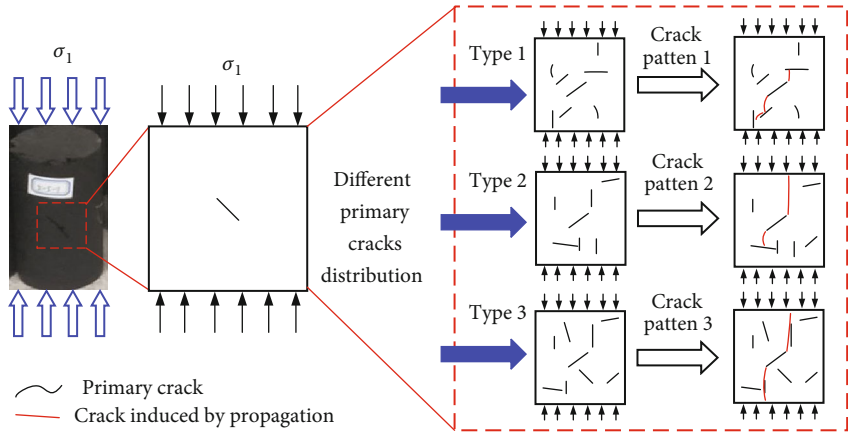

Figure 9: Crack propagation with different primary crack distributions.

around the tips of the flaw. When the stress concentration exceeded the local strength of the material, numerous microcracks were generated around the flaw. As the compressive load increased, the microcracking activity increased and gradually clustered into macroscopic cracks. With increasing stress, the macroscopic cracks expanded along the direction of maximum principal stress, that is, the uniaxial loading direction. In the process of microcrack connection and macroscopic crack propagation, the nonuniform distribution of primary cracks in coal has an important effect on crack propagation. When the direction of the crack propagation is close to that of the primary crack, the energy required for crack propagation is significantly reduced. This implies that a smaller stress increment is required for crack propagation, as shown in Figure 9. This explains why there was no specific change law for the strengths of fractured specimens with different fissure angles.

4.2. Guidance for Field Application. Figure 10 depicts the failure modes and sketches of the specimens with different fissure angles. When the fissure angle was 0°, axial crack propagation occurred, and the specimen broke. When the

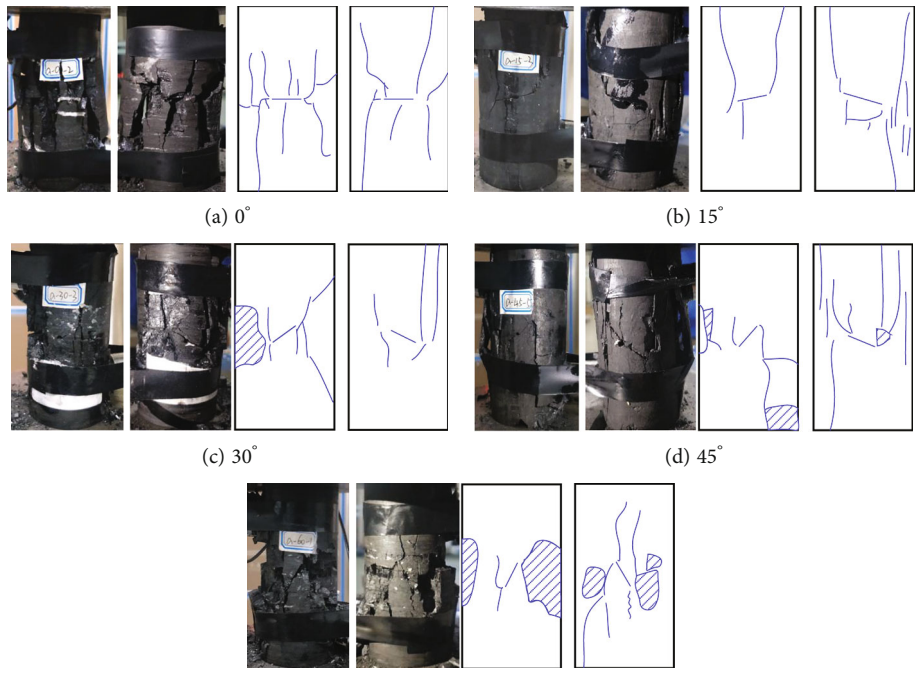

(a) 0° (b) 15° (c) 30° (d) 45° (e) 60°

Figure 10: Failure modes and sketches of specimens with different fissure angles.

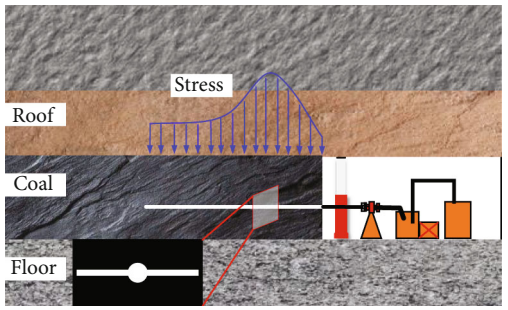

Figure 11: Typical hydraulic slotting in a coal mine.

fissure angle increased to 15°, more macroscopic cracks were produced in the specimen, but the number of cracks was reduced compared to that at 0°. As the fissure angle continued to increase, for example, to 30°, 45°, and 60°, numerous macroscopic cracks were generated on the specimen surface, and dynamic phenomena such as particle and block ejection occurred during the failure process. This indicates that with an increase in the fissure angle, the number of macroscopic cracks decreased, and dynamic phenomena (particle and block ejection) occurred.

Hydraulic slotting technology can enhance the drainage effect of gas and adjust the stress distribution of a coal body; thus, it has a wide range of field applications [45]. As an uneven geological body, coal seams contain abundant primary cracks. After hydraulic slotting, cracks were initiated and developed around the slots under the action of the stress field, as shown in Figure 11. According to the results of this study, a slot with a small fissure angle should be set to promote the development of cracks and prevent the emergence of dynamic phenomena.

The coal used in this study was relatively hard (uniaxial compressive strength of approximately 32.8 MPa) and had a high impact tendency, which explains the dynamic phenomena during the failure process. The authors plan to experimentally and numerically investigate the effects of stress state, coal quality, and multiple defects on the mechanical properties of coal specimens to enhance the present understanding of the mechanical properties and crack propagation behavior of fractured coal.

5. Conclusions

(1) The stress–strain behavior of the fractured specimens was divided into four typical stages: compaction, elastic deformation, crack growth and propagation, and strain softening. Preexisting fissures reduced the duration of the elastic stage and significantly affected the morphologies of the specimens during the crack growth and propagation stage and strain-softening stages. The uniaxial compressive strengths and elastic moduli of the specimens containing preexisting fissures were lower than those of intact specimens. The strengths and elastic moduli exhibited no specific trend with an increase in the fissure angle

(2) The stress–strain curves accurately reflected the macroscopic crack growth of the fractured specimens, and the stress drop generally corresponded to significant macroscopic crack growth. The fissure angle significantly affects the initiation location of the first crack. When the fissure angle was 0°, a crack formed at the centre of the preexisting fissure. With

an increase in the fissure angle, the initiation location moves to the tip of the fissure. The crack propagation direction, which developed along the loading direction, was unaffected by the fissure angle

(3) AE characteristics can be divided into three typical periods: calm, active, and remission. The AE counts and energy characteristics of the fractured specimens varied among different cracking stages. The duration proportion of the calm period increased with an increase in the fissure angle, indicating that the evolution characteristics of AE activities were different for different fissure angles

(4) According to an AE spectral frequency analysis and parameter analysis, AE signals were classified into five types: low-frequency–low-energy signals (L-L), low-frequency–high-energy signals (L-H), medium-frequency–low energy-signals (M-L), medium-frequency–high-energy signals (M-H), and high-frequency–low-energy signals (H-L). Low-frequency–high-energy signals (L-H signals) can be used to accurately predict the brittle fracture processes of fractured coals

(5) In contrast to rock specimens, the mechanical behaviors and failure mechanisms of coal specimens containing preexisting fissures are significantly affected by nonuniform primary cracks. The strength characteristics of the fractured specimens with different fissure angles did not exhibit a specific trend, which was attributed to the uneven distribution of the primary cracks inside the coal

Data Availability

The data used to support the findings of this study are available from the corresponding author upon reasonable request.

Disclosure

The paper was preprinted in research square with the doi:10.21203/rs.3.rs-870741/v1.

Conflicts of Interest

All authors declare that they have no conflict of interest.

Acknowledgments

The research described in this paper was financially supported by the Major Program of Shandong Provincial Natural Science Foundation (no. ZR2019ZD13), Major Scientific and Technological Innovation Project of Shandong Provincial Key Research Development Program (no. 2019SDZY02), National Natural Science Foundation of China (no. 51904165), and Taishan Scholar Engineering Construction Fund of Shandong Province of China (no. tsqn201812071).

References

[1] J. T. Chen, Y. Zhang, K. Ma, D. Z. Tang, H. Li, and C. X. Zhang, "Analysis of mining crack evolution in deep floor rock mass with fault," *Geofluids*, vol. 2021, Article ID 5583877, 15 pages, 2021.

[2] X. Lian, H. Hu, T. Li, and D. Hu, "Main geological and mining factors affecting ground cracks induced by underground coal mining in Shanxi Province, China," *International Journal of Coal Science and Technology*, vol. 7, no. 2, pp. 362–370, 2020.

[3] Y. Zong, L. Han, Q. Meng, and Y. Wang, "Strength properties and evolution laws of cracked sandstone samples in re-loading tests," *International Journal of Mining Science and Technology*, vol. 30, no. 2, pp. 251–258, 2020.

[4] X. Hao, W. Du, Y. Zhao et al., "Dynamic tensile behaviour and crack propagation of coal under coupled static-dynamic loading," *International Journal of Mining Science and Technology*, vol. 30, no. 5, pp. 659–668, 2020.

[5] T. Zhao, M. Xing, W. Guo, C. Wang, and B. Wang, "Anchoring effect and energy-absorbing support mechanism of large deformation bolt," *Journal of Central South University*, vol. 28, no. 2, pp. 572–581, 2021.

[6] Y. Tan, W. Guo, H. Xin, T. Zhao, F. Yu, and X. Liu, "Key technology of rock burst monitoring and control in deep coal mining," *Journal of China Coal Society*, vol. 44, no. 1, pp. 160–172, 2019.

[7] Y. Tan, W. Guo, T. Zhao, and X. Meng, "Coal rib burst mechanism in deep roadway and "stress relief-support reinforcement" synergetic control and prevention," *Journal of China Coal Society*, vol. 45, no. 1, pp. 66–81, 2020.

[8] T. B. Zhao, P. F. Zhang, W. Y. Guo, Y. X. Xiao, Y. Q. Zhao, and X. Sun, "Research on mechanical properties and acoustic emission characteristics of rock beams with different lithologies and thicknesses," *Latin American Journal of Solids and Structures*, vol. 18, no. 8, 2021.

[9] Q. Liu, J. Xu, X. Liu, J. Jiang, and B. Liu, "The role of flaws on crack growth in rock-like material assessed by AE technique," *International Journal of Fracture*, vol. 193, no. 2, pp. 99–115, 2015.

[10] J. Tian, D. Xu, and T. Liu, "An experimental investigation of the fracturing behaviour of rock-like materials containing two V-shaped parallelogram flaws," *International Journal of Mining Science and Technology*, vol. 30, no. 6, pp. 777–783, 2020.

[11] Y. Wang and C. Li, "Investigation on crack coalescence behaviors for granite containing two flaws induced by cyclic freeze-thaw and uniaxial deformation in Beizhan Iron Mining, Xinjing, China," *Geofluids*, vol. 2020, Article ID 7016823, 19 pages, 2020.

[12] J. Z. Zhang and X. P. Zhou, "AE event rate characteristics of flawed granite: from damage stress to ultimate failure," *Geophysical Journal International*, vol. 222, no. 2, pp. 795–814, 2020.

[13] L. N. Y. Wong and H. H. Einstein, "Crack coalescence in molded gypsum and Carrara marble: part 1. Macroscopic observations and interpretation," *Rock Mechanics and Rock Engineering*, vol. 42, no. 3, pp. 475–511, 2009.

[14] L. N. Y. Wong and H. H. Einstein, "Crack coalescence in molded gypsum and Carrara marble: part 2—microscopic observations and interpretation," *Rock Mechanics and Rock Engineering*, vol. 42, no. 3, pp. 513–545, 2009.

[15] S. Yang and H. Jing, "Strength failure and crack coalescence behavior of brittle sandstone specimens containing a single fissure under uniaxial compression," *International Journal of Fracture*, vol. 168, no. 2, pp. 227–250, 2011.

[16] S. P. Morgan, C. A. Johnson, and H. H. Einstein, "Cracking processes in Barre granite: fracture process zones and crack coalescence," *International Journal of Fracture*, vol. 180, no. 2, pp. 177–204, 2013.

[17] L. Dou, K. Yang, and X. Chi, "Fracture behavior and acoustic emission characteristics of sandstone specimens with inclined precracks," *International Journal of Coal Science and Technology*, vol. 8, no. 1, pp. 77–87, 2021.

[18] X. P. Zhou, J. Z. Zhang, Q. H. Qian, and Y. Niu, "Experimental investigation of progressive cracking processes in granite under uniaxial loading using digital imaging and AE techniques," *Journal of Structural Geology*, vol. 126, pp. 129–145, 2019.

[19] H. Haeri, K. Shahriar, M. F. Marji, and P. Moarefvand, "Experimental and numerical study of crack propagation and coalescence in pre-cracked rock-like disks," *International Journal of Rock Mechanics and Mining Sciences*, vol. 67, pp. 20–28, 2014.

[20] L. Yu, Q. Yao, Q. Xu, W. Wang, Z. Niu, and W. Liu, "Experimental and numerical simulation study on crack propagation of fractured fine sandstone under the influence of loading rate," *Journal of China Coal Society*, vol. 46, no. 11, pp. 3488–3501, 2021.

[21] T. Xiao, X. Li, and S. Jia, "Failure characteristics of rock with two pre-existing transfixion cracks under triaxial compression," *Chinese Journal of Rock Mechanics and Engineering*, vol. 34, no. 12, pp. 2455–2462, 2015.

[22] Y. Huang and S. Yang, "Particle flow simulation of macro- and meso-mechanical behavior of red sandstone containing two pre-existing non-coplanar fissures," *Chinese Journal of Rock Mechanics and Engineering*, vol. 33, no. 8, pp. 1644–1653, 2014.

[23] X. Wang, P. Yu, X. Zhang et al., "Simulation of three-dimensional tension-induced cracks based on cracking potential function-incorporated extended finite element method," *Journal of Central South University*, vol. 28, no. 1, pp. 235–246, 2021.

[24] S. Yu, X. Ren, J. Zhang, H. Wang, and Z. Sun, "An improved form of smoothed particle hydrodynamics method for crack propagation simulation applied in rock mechanics," *International Journal of Mining Science and Technology*, vol. 31, no. 3, pp. 421–428, 2021.

[25] X. P. Zhou, J. Z. Zhang, S. Q. Yang, and F. Berto, "Compression-induced crack initiation and growth in flawed rocks: a review," *Fatigue & Fracture of Engineering Materials & Structures*, vol. 44, no. 7, pp. 1681–1707, 2021.

[26] M. Bahaaddini, G. Sharrock, and B. K. Hebblewhite, "Numerical investigation of the effect of joint geometrical parameters on the mechanical properties of a non-persistent jointed rock mass under uniaxial compression," *Computers and Geotechnics*, vol. 49, pp. 206–225, 2013.

[27] L. N. Y. Wong and H. Li, "Numerical study on coalescence of two pre-existing coplanar flaws in rock," *International Journal of Solids and Structures*, vol. 50, no. 22-23, pp. 3685–3706, 2013.

[28] J. Lee, J. Hong, and J. Jung, "The mechanism of fracture coalescence in pre-cracked rock-type material with three flaws," *Engineering Geology*, vol. 223, pp. 31–47, 2017.

[29] C. Zhao, Y. M. Zhou, C. F. Zhao, and C. Bao, "Cracking processes and coalescence modes in rock-like specimens with two parallel pre-existing cracks," *Rock Mechanics and Rock Engineering*, vol. 51, no. 11, pp. 3377–3393, 2018.

[30] S. Huang, N. Yao, Y. C. Ye, and X. Z. Cui, "Strength and failure characteristics of rocklike material containing a large-opening crack under uniaxial compression: experimental and numerical studies," *International Journal of Geomechanics*, vol. 19, no. 8, 2019.

[31] Y. L. Wang, J. X. Tang, Z. Y. Dai, T. Yi, and X. Y. Li, "Effect of fracture number and aperture on mechanical properties and failure modes of low-strength rock mass," *Journal of China Coal Society*, vol. 43, no. 12, pp. 3338–3347, 2018.

[32] T. J. Zhang, H. L. Guo, C. Jing, L. Zhang, and K. Wang, "Mechanism of meso-crack damage evolution in failure process of porous soft coal specimens," *Coal Science and Technology*, vol. 49, no. 12, pp. 96–103, 2021.

[33] T. J. Zhang, X. N. Wang, C. Jing, L. Zhang, H. Y. Pan, and S. Zhang, "Localized deformation characteristics of soft coal with fractures at different dip angles," *Journal of Xi'an University of Science and Technology*, vol. 41, no. 2, pp. 203–212, 2021.

[34] T. Jin and Q. W. Lian, "Numerical simulation study on effect of fracture angle on coal impact tendency," *Coal Technology*, vol. 41, no. 5, pp. 125–128, 2022.

[35] W. Liu and J. Shen, "Experimental study of propagation mode of crack in real rock specimens with a single crack," *Chinese Journal of Rock Mechanics and Engineering*, vol. 35, no. 6, pp. 1182–1189, 2016.

[36] W. Guo, D. Zhang, T. Zhao et al., "Influence of rock strength on the mechanical characteristics and energy evolution law of gypsum–rock combination specimen under cyclic loading–unloading condition," *International Journal of Geomechanics*, vol. 22, no. 5, 2022.

[37] Y. Du, G. Feng, H. Kang et al., "Investigation on the mechanical behavior and failure characteristics of fully grouted bolts under tension," *Energy Sources, Part A: Recovery, Utilization, and Environmental Effects*, pp. 1–15, 2020.

[38] Z. Huang, Q. Gu, Y. Wu et al., "Effects of confining pressure on acoustic emission and failure characteristics of sandstone," *International Journal of Mining Science and Technology*, vol. 31, no. 5, pp. 963–974, 2021.

[39] G. Su, W. Gan, S. Zhai, and G. Zhao, "Acoustic emission precursors of static and dynamic instability for coarse-grained hard rock," *Journal of Central South University*, vol. 27, no. 10, pp. 2883–2898, 2020.

[40] Y. Guo, Y. Zhao, S. Wang, G. Feng, Y. Zhang, and H. Ran, "Stress-strain-acoustic responses in failure process of coal rock with different height to diameter ratios under uniaxial compression," *Journal of Central South University*, vol. 28, no. 6, pp. 1724–1736, 2021.

[41] C. Wang, Z. Chen, Z. Liao et al., "Experimental investigation on predicting precursory changes in entropy for dominant frequency of rockburst," *Journal of Central South University*, vol. 27, no. 10, pp. 2834–2848, 2020.

[42] Q. Zou, H. Liu, Z. Jiang, and X. Wu, "Gas flow laws in coal subjected to hydraulic slotting and a prediction model for its permeability-enhancing effect," *Energy Sources, Part A: Recovery, Utilization, and Environmental Effects*, pp. 1–15, 2021.

[43] J. Z. Zhang, X. P. Zhou, L. S. Zhou, and F. Berto, "Progressive failure of brittle rocks with non-isometric flaws: insights from

acousto-optic-mechanical (AOM) data," *Fatigue & Fracture of Engineering Materials & Structures*, vol. 42, no. 8, pp. 1787–1802, 2019.

[44] X. P. Zhou, H. Cheng, and Y. F. Feng, "An experimental study of crack coalescence behaviour in rock-like materials containing multiple flaws under uniaxial compression," *Rock Mechanics and Rock Engineering*, vol. 47, no. 6, pp. 1961–1986, 2014.

[45] X. P. Zhou and J. Z. Zhang, "Damage progression and acoustic emission in brittle failure of granite and sandstone," *International Journal of Rock Mechanics and Mining Sciences*, vol. 143, article 104789, 2021.